A Line-Free Discrete Dislocation Dynamics Method for Finite Domains

Aitor Cruzado, Pilar Ariza, Alan Needleman, Michael Ortiz, and Amine Benzerga

Abstract A method for solving general boundary-value problems involving discrete dislocations is introduced. Plastic flow emerges from the motion of dislocations in an incremental fashion. At each increment, the displacement, strain and stress fields in the body are obtained by superposition of the infinite medium fields associated with individual dislocations and an image field that enforces boundary conditions. Dislocations are represented as monopoles and dislocation events are treated as a transportation map problem. Long-range interactions are accounted for through linear elasticity with a core regularization procedure. At the current state of development of the method, no ad hoc short-range interactions are included. An approximate loop nucleation model is used for large-scale computations. The image problem is solved using a finite element formulation with the following features: (i) a single Cholesky decomposition of the global stiffness matrix, (ii) a consistent enforcement of traction and displacement boundary conditions, and (iii) image force interpolation using an efficient BB-tree algorithm. To ensure accuracy, we explore stable time steps and employ monopole splitting techniques. Special attention is given to the interaction of curved dislocations with arbitrary domain boundaries and free surfaces. The capabilities of the framework are illustrated through a wire torsion problem.

Keywords DDD · Line free method · Free surfaces · Finite elements

A. Cruzado (✉) · A. Benzerga
Department of Aerospace Engineering, Texas A&M University, College Station, TX 77843, USA
e-mail: aitor.cruzado@tamu.edu

P. Ariza
Escuela Técnica Superior de Ingeniería, Universidad de Sevilla, 41092 Sevilla, Spain

A. Needleman · A. Benzerga
Department of Materials Science & Engineering, Texas A&M University, College Station, TX 77843, USA

M. Ortiz
Division of Engineering and Applied Science, California Institute of Technology, Pasadena, CA 91125, USA

The Minerals, Metals & Materials Society (ed.), *TMS 2024 153rd Annual Meeting & Exhibition Supplemental Proceedings*, The Minerals, Metals & Materials Series,
https://doi.org/10.1007/978-3-031-50349-8_71

Introduction

Nearly three decades ago, discrete dislocation plasticity [1] emerged as a powerful framework for dealing with a range of problems where microstructural and dimensional length scales strongly interact. Phenomena analyzed within this framework include size effects [2, 3], fatigue [4], strain hardening [5], grain-size strengthening [6] creep [7, 8], and elastodynamics [9]. The framework is, however, limited to edge dislocations within a plane strain two-dimensional setting. Alternatively, three-dimensional dislocation dynamics methods have been developed with increasing sophistication [10–13], but for the most part have remained limited to infinite domains, e.g. under the assumption of periodicity. Methods that have been developed for finite domains [14–17] involve computationally inefficient coupling with finite elements and tedious constraints for maintaining linear connectivity among dislocation segments due to the line-based character of the methods.

Recently, a line-free method has been developed which is based on the notion of monopoles [18]. Its simplicity resides in the point-like character of monopoles, which does not require keeping track of connectivity. A monopole represents a discrete element of line dislocations, each carrying a Burgers vector. Monopoles exhibit mobility kinetics driven by a synergy of elastic interactions and externally applied forces, allowing them to replicate the dynamic behavior of dislocations. The method has recently been used to investigate hardening in nano-crystals [19]. The purpose of this paper is to expand upon this method and develop a fully consistent coupling with finite elements to solve boundary value problems in arbitrary domains for small deformations.

Formulation

A finite body occupying domain Ω is subjected to boundary tractions $\mathbf{T}_0$ and boundary displacements $\mathbf{U}_0$ on boundary parts $\partial\Omega_\mathrm{t}$ and $\partial\Omega_\mathrm{u}$, respectively. The body contains dislocation loops each being discretely represented by a set of monopoles $a = 1 \cdots M$ with coordinates $\{\mathbf{x}_a\}_{a=1}^{M}$. Following the line-free method of monopoles for 3D dislocation dynamics [18, 19] each monopole concentrates a dislocation line density and carries a Burgers vector $\{\mathbf{b}_a\}_{a=1}^{M}$ and element of line $\{\boldsymbol{\xi}_a\}_{a=1}^{M}$.

At time t the body is in equilibrium and the position of each monopole in the body is known. Superposition is used as in [1] to write the displacement rate $\dot{\mathbf{u}}$, strain, $\boldsymbol{\varepsilon}$, and stress, $\boldsymbol{\sigma}$, fields as:

$$\dot{\mathbf{u}}(\mathbf{x}) = \tilde{\dot{\mathbf{u}}}(\mathbf{x}) + \hat{\dot{\mathbf{u}}}(\mathbf{x}) \quad ; \quad \boldsymbol{\varepsilon} = \tilde{\boldsymbol{\varepsilon}} + \hat{\boldsymbol{\varepsilon}} \quad ; \quad \boldsymbol{\sigma} = \tilde{\boldsymbol{\sigma}} + \hat{\boldsymbol{\sigma}}, \tag{1}$$

where the $\tilde{(\cdot)}$ fields are obtained by superposition of the infinite medium fields of individual dislocation loops and the $\hat{(\cdot)}$ fields are image fields that enforce the boundary conditions. Formally, one may write:

$$\tilde{\boldsymbol{\sigma}}(\mathbf{x}) = \sum_{a=1}^{M} \boldsymbol{\sigma}_a(\mathbf{x}) \tag{2}$$

where $\boldsymbol{\sigma}_a(\mathbf{x})$ is a term arising from using an appropriate Green's function and Mura's formula [20] for a general loop in a homogeneous unbounded medium. Details on stress calculations will be given elsewhere. For example, the time- and monopole-discretized infinite medium displacements read:

$$\mathbf{u}_{v+1}(\mathbf{x}) - \mathbf{u}_v(\mathbf{x}) = \sum_{a=1}^{M} \boldsymbol{\sigma}^{\epsilon}(\mathbf{x} - \mathbf{x}_{a,v+1/2}) \cdot \mathbf{b}_{a,v+1/2} \otimes \boldsymbol{\xi}_{a,v+1/2} \times (\mathbf{x}_{a,v+1} - \mathbf{x}_{a,v}) \tag{3}$$

where Σ^{ϵ}_{ijk} is the stress corresponding to a regularized Green's function G^{ϵ}_{ij}. For isotropic elasticity with Lamé constants λ and μ,

$$\boldsymbol{\sigma}^{\epsilon}_{ijk} = \lambda G^{\epsilon}_{ip,p}\delta_{jk} + \mu(G^{\epsilon}_{ij,k} + G^{\epsilon}_{ik,j}) \tag{4}$$

On the other hand, the $\hat{(\cdot)}$ fields are governed by a linear elastic boundary value problem:

$$\nabla \cdot \hat{\boldsymbol{\sigma}} = \mathbf{0} \quad ; \quad \hat{\varepsilon} = \nabla \otimes \hat{\mathbf{u}} \quad ; \quad \hat{\boldsymbol{\sigma}} = \boldsymbol{\mathcal{L}} : \hat{\varepsilon} \qquad \text{for } \mathbf{x} \in \Omega, \tag{5}$$

$$\mathbf{n} \cdot \hat{\boldsymbol{\sigma}} = \mathbf{T}_0 - \mathbf{n} \cdot \tilde{\boldsymbol{\sigma}} \quad \text{for } \mathbf{x} \in \partial\Omega_{\mathrm{t}} \quad ; \quad \hat{\mathbf{u}} = \mathbf{U}_0 - \tilde{\mathbf{U}} \quad \text{for } \mathbf{x} \in \partial\Omega_{\mathrm{u}} \tag{6}$$

with $\boldsymbol{\mathcal{L}}$ the isotropic tensor of elastic moduli and $\mathbf{n}$ the outer normal.

The method employed here does not require direct (and costly) traction calculations on the surface. Instead, if $\mathbf{F}_{0,\mathrm{n}}$ denote the imposed nodal forces on a set Γ_{f} of boundary nodes, $\hat{\mathbf{f}}_{\mathrm{n}}$ and $\tilde{\mathbf{f}}_{\mathrm{n}}$ the corresponding nodal forces for the $\hat{(\cdot)}$ and $\tilde{(\cdot)}$ problems, respectively, i.e.

$$\hat{\mathbf{f}}_{\mathrm{n}} = \mathbf{F}_{0,\mathrm{n}} - \tilde{\mathbf{f}}_{\mathrm{n}}, \qquad \mathrm{n} \in \Gamma_{\mathrm{f}}, \tag{7}$$

then the tilde forces are assembled over all elements that share a boundary surface node (total number N_{el}):

$$\tilde{\mathbf{f}}_{\mathrm{n}} = \sum_{e=1}^{N_{\mathrm{el}}} \tilde{\mathbf{f}}_e \qquad \mathrm{n} \in \Gamma_{\mathrm{f}} \tag{8}$$

where $\tilde{\mathbf{f}}_e$ is determined through consistent per element integration of the infinite-medium stresses (number of integration points N_{ip}):

$$\tilde{\mathbf{f}}_{\mathrm{e}} = \sum_{i=1}^{N_{\mathrm{ip}}} \boldsymbol{B}^{\boldsymbol{T}}(\xi_i, \eta_i, \zeta_i)\tilde{\boldsymbol{\sigma}}(\xi_i, \eta_i, \zeta_i)\,|\boldsymbol{J}_i|\,w_i \tag{9}$$

Here, $\boldsymbol{B}^{\boldsymbol{T}}$ are the shape function "derivatives" evaluated at integration point (ξ_i, η_i, ζ_i), $|\boldsymbol{J}_i|$ is the determinant of the Jacobian and w_i the weight of i.

The motion of a monopole is driven by the Peach-Koehler force:

$$\mathbf{f}_a = \hat{\boldsymbol{\sigma}}(\mathbf{x}_a) \cdot \mathbf{b}_a \times \boldsymbol{\xi}_a + \sum_{b \neq a}^{M} \boldsymbol{\sigma}_b(\mathbf{x}_a) \cdot \mathbf{b}_a \times \boldsymbol{\xi}_a \tag{10}$$

The first term corresponds to the externally applied force, denoted $\mathbf{f}_a^{\text{ext}}$ in [19]. The second term is replaced with $\mathbf{f}_a^{\epsilon}$, which accounts for core regularization. The complete expression can be found in [18, 19]. Here, only the glide component is considered. The current position of monopole a is obtained by solving the implicit Euler-Lagrange equation:

$$D\psi(\mathbf{v}_a(t)) \left|\boldsymbol{\xi}_a(t)\right| + \mathbf{f}_a^{\epsilon}(\mathbf{x}(t)) + \mathbf{f}_a^{\text{ext}}(\mathbf{x}(t)) = 0, \tag{11}$$

where $\mathbf{v}_a$ is the monopole velocity, $D\psi(\mathbf{v}_a(t))$ denotes partial differentiation of the kinetic potential, here defined by a linear mobility law of the form:

$$\psi\left(\mathbf{v}_a(t)\right) = \frac{1}{2M} \left|\mathbf{v}_a(t)\right|^2, \tag{12}$$

with M the mobility. The elements of line are updated explicitly by the local gradient of the incremental transport map:

$$\dot{\boldsymbol{\xi}}_a(t) = \sum_{b=1}^{M} (\nabla N_b(\mathbf{x}_a, t) \cdot \boldsymbol{\xi}_a(t)) \mathbf{v}_b(t), \tag{13}$$

where the mesh-free scheme for the interpolation of the velocity is specified using the Max-ent shape functions:

$$N_a(\mathbf{x}, t) = \frac{1}{Z} \exp\left(-\frac{\beta_a}{2} |\mathbf{x} - \mathbf{x}_a(t)|^2\right), \quad Z = \sum_{a=1}^{M} \exp\left(-\frac{\beta_a}{2} |\mathbf{x} - \mathbf{x}_a(t)|^2\right), \tag{14}$$

These shape functions "connect" the monopoles through an effective interaction distance of $1/\sqrt{\beta}$. Time integration of Eqs. (11) and (13) is accomplished using an explicit two-stage Runge–Kutta method [19] or the Polak–Ribière iterative solver [18].

Determining the first term in Eq. (10), $\mathbf{f}_a^{\text{ext}}$, requires evaluating the image stress, determined by solving Eqs. (5) and (6), at the location of monopole a. This is accomplished by interpolating the $\hat{\boldsymbol{\sigma}}$ field. In the course of a simulation, monopoles change elements. An efficient BB-tree element locator is used, given monopole coordinates $\mathbf{x}_a$. Since the $\hat{\boldsymbol{\sigma}}$ field is discontinuous across element boundaries, it is first extrapolated to element nodes through the shape functions. Then the nodal values are averaged over all elements sharing the same node, before interpolation to the monopoles.

Next, the interaction of monopoles with free surfaces is treated as follows. The infinite medium analytical expression for $\tilde{\boldsymbol{\sigma}}$ is only valid for a dislocation loop. If part of the loop exits the body spurious stresses may be evaluated on the surface. To address this, a method of virtual monopoles is introduced, which mimics virtual segments in line-based methods. Thus, the monopoles that now lie outside of Ω are detected (using a BB-tree) and removed. The two monopoles that are closest to the surface are identified and virtual monopoles are introduced to close the loop for subsequent stress calculations.

The evolution problem is approached incrementally, demanding an efficient code coupling strategy. The MonoDis code [18, 19] is fully integrated within the finite element software Z-set [21] through a plug-in interface. Inversion of the global stiffness matrix is executed *once*, resulting in minimal computational burden in FEM. The methodology involves the following steps:

1. At time t the body is in equilibrium and the position of each monopole in the body is known. The surface nodal forces $\tilde{\mathbf{f}}$ derived from $\tilde{\boldsymbol{\sigma}}$ and displacements $\tilde{\boldsymbol{u}}$ are computed.
2. The boundary-value problem defined by Eqs. (5) and (6) for the $\hat{\boldsymbol{\sigma}}$ field is solved.
3. The $\hat{\boldsymbol{\sigma}}$ field is interpolated to monopole locations in order to evaluate the Peach-Koehler forces.
4. The mobility problem, Eq. (11), is solved to determine new monopole positions at time $t + \Delta t$.
5. Monopoles that lie outside the body are flagged and removed. Virtual monopoles are added to close the dislocation loop for stress calculations.
6. Go to 1: $t \leftarrow t + \Delta t$.

In this process, a distinctive rule involves modeling loop nucleation by introducing circular general loops. Locations of initial potential sources are randomly distributed in the body. At a given source location, a loop of radius ρ nucleates when $\|\mathbf{f}_a^{ext}\| > \|\mathbf{f}_a^{\epsilon}\|$ where $a = \arg\max_{\mathrm{n}}(\|\mathbf{f}_n^{\epsilon}\|)$ is the monopole that presents the maximum regularized linear elastic PK force.

Results

We first explore the optimal element of line ξ that reproduces the non-singular solution for prismatic loops [18] and general loops [22]. For a core regularization parameter of $\epsilon = b$, we find that a value $\xi = 0.43b$ is needed to recover the analytical solution of the prismatic loop, Fig. 1a. A scalability relation between ξ and ϵ is also determined, which enables calculations with larger elements of lines without sacrificing accuracy. The relationship only holds for sufficiently large loops.

To illustrate free surface effects, we consider, as in [14], a circular loop with radius $r = 4000a$ and Burgers vector $\mathbf{b} = a(100)/\sqrt{2}$ placed at the center of a cube

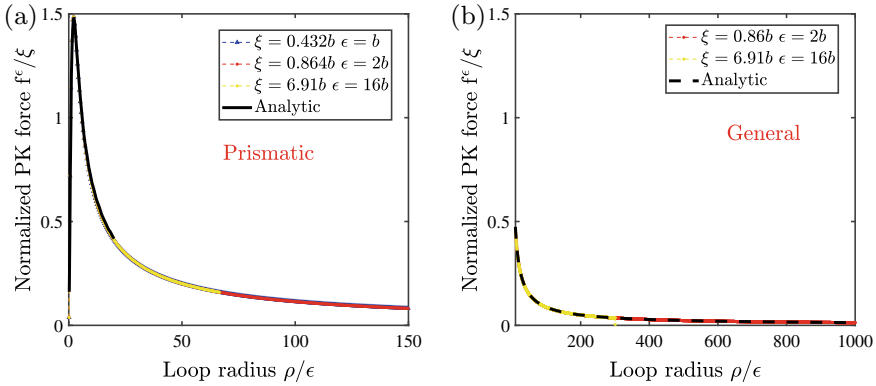

Fig. 1 Peach-Koehler force (per unit length) normalized by $\mu b^2/(8\pi(1-\nu)\epsilon)$ versus loop radius for: **a** prismatic loops and **b** general loops

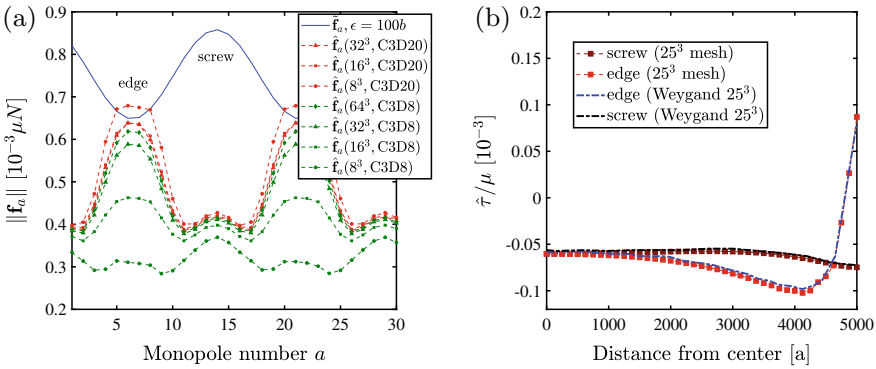

Fig. 2 **a** Glide PK force around the loop for various FE mesh discretizations. **b** Image shear stress, $\hat{\tau}$, versus distance from center of loop

with traction free boundary conditions and parallel to (010) face. The cube has side length $L = 10000a$ and Cu material properties: lattice parameter $a = 0.3614$ nm, shear modulus $\mu = 45$ GPa, mobility $M = 5.56 \times 10^{21}$ nm^2/Ns. Figure 2a shows both the analytically known infinite medium PK force (blue) and the FE computed image force for two types of finite elements and various mesh densities.

Using quadratic elements, convergence is attained for a mesh density of 16^3 elements (element size of $441b$). Furthermore, we verify that the hat component of the resolved shear stress, $\hat{\tau} = -n_i\hat{\sigma}_{ij}b_j/b$, corresponds to the numerical solution obtained in [14] using a line-based method, Fig. 2b.

Next, consider the nucleation criterion. If the loop radius at nucleation is taken to coincide with the annihilation radius $\rho_0 = 2.25\epsilon$ (from maximum PK force in Fig. 2), then the corresponding equilibrium resolved shear stress is $\tau_{\text{nuc}} = f^{\epsilon}\rho_0/(\boldsymbol{\xi}b)$. Stable growth of dislocation loops occurs when they nucleate at $\tau = 1.5\tau_{nuc}$, as depicted in

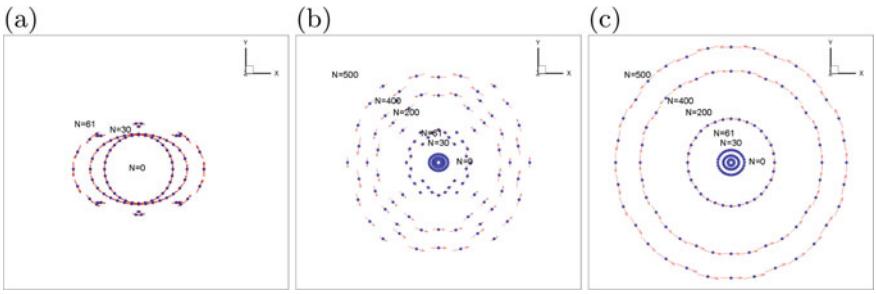

Fig. 3 Analysis of stable growth of nucleated loops for an applied stress **a** $\tau = \tau_{\text{nuc}}$, **b** $\tau = 1.25\tau_{\text{nuc}}$ and **c** $\tau = 1.5\tau_{\text{nuc}}$

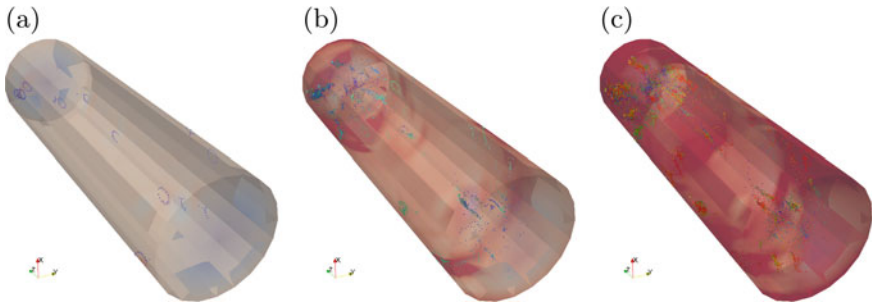

Fig. 4 Dislocation network evolution in a Cu wire measuring 500 nm in diameter and 1750 nm in length subjected to a twist of: **a** 1°, **b** 1.5° and **c** 2°

Fig. 3c. However, stable simulations require time increments $\Delta t \approx 10^{-14}$. If loops with a radius of operation of Frank–Read sources, say $\rho > 100b$ and $\epsilon \approx 20b$, are nucleated, stable simulations are possible with $\Delta t \approx 10^{-10} - 10^{-9}s$.

Finally, we illustrate the dislocation network evolution in a wire under torsion oriented for single slip and initially containing 50 sources each with a nucleation radius $\rho = 30$nm, Fig. 4. The wire's diameter is $d = 500$ nm with aspect ratio $l/d = 3.5$. We verify the early activation of sources located near the surface due to higher shear stresses, Fig. 4a. As the twist increases, the dislocation network evolves with dislocation loops enlarging and parts exiting the wire, Fig. 4b. At a 2° twist, Fig. 4c, monopoles are notably trapped near the wire's center, as expected. An analysis of size effects is underway.

Concluding Remarks

A 3D discrete dislocation plasticity framework is under development, enabling dislocation dynamics in diverse domains for small deformations. This framework employs

the MonoDis code as a basis for treating dislocation dynamics using monopoles, while the Z-set software employs finite elements to solve the image problem. Notable features include a single Cholesky decomposition of the global stiffness matrix, a consistent enforcement of boundary conditions, a virtual monopole technique for dislocation-free surface interactions, and an approximate nucleation model for efficient large-scale computations at a reasonable time step (>0.1 ns).

Acknowledgements AAB acknowledges support from NSF under grant CMMI-1950027. AC and AAB thank Vincent Chiaruttini and Jean-Didier Garaud from ONERA for assistance with the plugin interface of Z-set.

References

1. Van der Giessen E, Needleman A (1995) Modell Simul Mater Sci Eng 3:689–735
2. Nicola L, Van der Giessen E, Needleman A (2003) J Appl Phys 93:5920–5928
3. Guruprasad PJ, Benzerga AA (2008) J Mech Phys Solids 56:132–156
4. Deshpande VS, Needleman A, Van der Giessen E (2001) Acta Mater 49:3189
5. Benzerga AA, Bréchet Y, Needleman A, Van der Giessen E (2004) Modell Simul Mater Sci Eng 12:159–196
6. Balint DS, Deshpande VS, Needleman A, Van der Giessen E (2008) Int J Plast 24:2149–2172
7. Keralavarma SM, Cagin T, Arsenlis A, Benzerga AA (2012) Phys Rev Lett 109:265504
8. Shishvan SS, McMeeking RM, Pollock TM, Deshpande VS (2017) Acta Mater 135:188–200
9. Gurrutxaga-Lerma B, Balint DS, Dini D, Sutton AP (2015) Proc R Soc A 471:20150433
10. Devincre B, Kubin L (1997) Mater Sci Eng 8(14):234–236
11. Zbib H, Rhee M, Hirth JP (1998) Int J Mech Sci 40:113–127
12. Ghoniem NM, Sun LZ (1999) Phys Rev B 60:128–140
13. Arsenlis A, Cai W, Tang M, Rhee M, Oppelstrup T, Hommes G, Pierce TG, Bulatov VV (2007) Modell Simul Mater Sci Eng 15(6):553–595
14. Weygand D, Friedman LH, Van der Giessen E, Needleman A (2002) Modell Simul Mater Sci Eng 10:437–468
15. Crone JC, Chung PW, Leiter KW, Knap J, Aubry S, Hommes G, Arsenlis A (2014) Modell Simul Mater Sci Eng 22(3):035014 Mar
16. Vattré A, Devincre B, Feyel F, Gatti R, Groh S, Jamond O, Roos A (2014) J Mech Phys Solids 63:491–505
17. Ryu Ill, Gravell JD, Cai W, Nix WD, Gao H (2020) Extreme Mech Lett 40:100901
18. Deffo A, Ariza MP, Ortiz M (2019) J Mech Phys Solids 122:566–589
19. Ariza MP, Ortiz M (2021) Extreme Mech Lett 45:101267
20. Mura T (1982) Micromechanics of defects in solids. Martinus Nijhoff Publishers
21. Z-set 9.1 package (2020) Non-linear material & structure analysis suite
22. Cai W, Arsenlis A, Weinberger CR, Bulatov V (2006) J Mech Phys Solids 54(3):561–587